An efficient C^1 finite element with continuity requirements for multilayered/sandwich shell structures

F. Dau [a,*], O. Polit [b], M.Touratier [c]

[a] *LAMEFIP, ENSAM, Esplanade des arts et métiers, 33405 Talence, France*
[b] *LMpX, 1 Chemin Desvallières, 92410 Ville d'Avray, France*
[c] *LMSP, UMR CNRS, ENSAM/ESEM, 151 Bd de l'Hopital, 75013 Paris, France*

Abstract

This paper deals with a new triangular finite element to analyze the behaviour of multilayered shells. This element is based on a refined kinematical model and uses both conforming finite element method and higher-order approximations. Including a nonlinear distribution with respect to the normal co-ordinate for the transverse shear stresses and continuity requirements between layers for both transverse shear stresses and displacements, this model does not require any shear correction factors. Moreover, it allows to satisfy the boundary conditions at the top and bottom surfaces of the shell. Various strain expressions available for shells are discussed. Although the program is able to calculate arbitrary shell shapes, present shell element performances are evaluated here in comparison with available analytical tests issued from literature. The present finite element shown very good responses on the classical shell test: pinched cylinder, pinched hemispherical shell, Scordelis–Lo roof. Finally, results in linear static, free vibrations and transient dynamic response for multilayered shells show the efficiency of this new shell finite element.

Keywords: Refined model; Transverse shear stresses; Multilayered shells; Interlayer and boundary continuity conditions; C^1 finite element

1. Introduction

Multilayered beam, plate and shell models are needed in structural mechanics for analyzing, dimensionning and designing this kind of structures, see for example the review paper [1]. In the field of multilayered shells where transverse shear stress effects are of great importance, many high-order shell theories exist, see for example [2–8], but few numerical tools have been developed.

In the recent literature, a layer-wise technique has been used to develop a triangle finite element based on condensation technique at the pre-processing level in order to reduce the computational cost [9]. A three-dimensional shell element is presented by Klinkel [10]. These numerical tools are not pure structural models and suffer of the classical shear and membrane lockings.

The aim of this work is to present a new finite element, simple to use, free from classical numerical

* Corresponding author. Fax: +33 5 56 84 53 35.
E-mail address: frederic.dau@lamef.bordeaux.ensam.fr (F. Dau).

doi:10.1016/j.compstruc.2003.10.026

pathologies and very efficient in computing both displacements and stresses for multilayered shell applications. This new C^1 shell finite element is based on the refined model given in [3] which incorporates:

- a cosine distribution for the transverse shear strains avoiding the use of shear correction factors;
- the continuity conditions between layers of the laminate for both displacements and transverse shear stresses;
- the satisfaction of the boundary conditions at the top and bottom surfaces of the shell;
- the use of only five independent generalized displacements (three translations and two rotations),

From a previous work on multilayered plate finite element [11], a new shell finite element has been developped using both conforming finite element method and high-order finite element approximations: Argyris interpolation for the transverse displacement and Ganev interpolation for membrane displacements and transverse shear rotations.

Some unavoidable geometric shell considerations are firstly presented to introduce necessary tools for shell description. In the second part of this paper, the shell model based on a refined kinematical approach is developed. The third part deals with different strain tensors which can be deduced from the displacement field. These shell models are evaluated using an analytical approach for a simply supported cylindrical shell panel under sinusoidal pressure. The next part is dedicated to finite element approximations corresponding to the above refined model. Finally, some linear static tests for multilayered plates and shells are described. Linear free vibration and transient dynamic responses are achieved in order to show the efficiency of this new finite element. It must be noticed that this efficiency is demonstrated for both convergence velocity and accuracy for displacements and stresses.

2. Geometric considerations

The shell $\mathscr{C}$ with a middle surface $\mathscr{S}$ and a constant thickness e is defined by:

$$\mathscr{C} = \left\{ M \in \mathscr{R}^3 : \vec{OM}(\xi,\xi^3) = \vec{\Phi}(\xi) + \xi^3\vec{a}_3; \xi \in \Omega; \right. \\ \left. -\frac{1}{2}e(\xi) \leqslant \xi^3 \leqslant \frac{1}{2}e(\xi) \right\}$$

where the middle surface is described by a map $\vec{\Phi}$ from a bidimensional domain Ω as:

$$\vec{\Phi} : \Omega \subset \mathscr{R}^2 \to \mathscr{S} \subset \mathscr{R}^3$$
$$\xi = (\xi^1,\xi^2) \mapsto \vec{\Phi}(\xi)$$

At any point of the shell middle surface, the covariant basis vectors are usually obtained as:

$$\vec{a}_\alpha = \vec{\Phi}(\xi)_{,\alpha}; \quad \vec{a}_3 = \frac{\vec{a}_1 \times \vec{a}_2}{\|\vec{a}_1 \times \vec{a}_2\|} \tag{1}$$

From these local covariant base vectors, coefficients of the first and second fundamental forms are deduced, and we have:

$$a_{\alpha\beta} = \vec{a}_\alpha \cdot \vec{a}_\beta$$
$$b_{\alpha\beta} = -\vec{a}_\alpha \cdot \vec{a}_{3,\beta} = \vec{a}_3 \cdot \vec{a}_{\beta,\alpha} \tag{2}$$

In Eq. (1) and further on, Latin indices $i,j,\ldots$ take their values in the set $\{1,2,3\}$, while Greek indices $\alpha,\beta,\ldots$ take their values in the set $\{1,2\}$. The summation convention on repeated indices and the classic notation $(\,)_{,\alpha} = \frac{\partial(\,)}{\partial\xi^\alpha}$ are used.

For any point of the shell, covariant base vectors are expressed as follow:

$$\vec{g}_\alpha = \vec{OM}(\xi,\xi^3)_{,\alpha} = (\delta^\beta_\alpha - \xi^3 b^\beta_\alpha)\vec{a}_\beta = \mu^\beta_\alpha \vec{a}_\beta \quad \text{and} \quad \vec{g}_3 = \vec{a}_3 \tag{3}$$

where curvature tensor is defined by b^β_α and δ^β_α is the Kronecker symbol. The mixed tensor m^β_α must also be introduced. It is defined by the relation:

$$m^\beta_\alpha = (\mu^{-1})^\beta_\alpha = \frac{1}{\mu}\{\delta^\beta_\alpha + \xi^3(b^\beta_\alpha - 2H\delta^\beta_\alpha)\} \tag{4}$$

where $\mu = \det(\mu^\beta_\alpha) = 1 - 2H\xi^3 + (\xi^3)^2K$; $H = \frac{1}{2}\mathrm{tr}(b^\beta_\alpha)$; $K = \det(b^\beta_\alpha)$.

Finally, the contravariant vectors are constructed from the covariant ones using the following equations:

$$\vec{a}^\alpha.\vec{a}_\beta = \delta^\alpha_\beta \quad \vec{a}^3 = \vec{a}_3; \quad \vec{g}^\alpha.\vec{g}_\beta = \delta^\alpha_\beta \quad \vec{g}^3 = \vec{g}_3 \tag{5}$$

All these relations are classic and it is not necessary to give more details in order to obtain the Christoffel's symbols and other differential geometric entities, see Bernadou [12].

3. The shell model

In order to define different shell models in this work, the displacement field is firstly introduced. Next, the methodology permitting to ensure interlayer continuity conditions and satisfaction of the boundary conditions at the top and bottom surfaces of the shell is presented. Finally, several strain models are presented according to some usual assumptions.

3.1. The displacement field

From Béakou and Touratier [13], the displacement field of a shell point, in each elastic layer denoted (k), is defined for a general doubly curved shell with respect to the contravariant base vectors $\vec{a}^i$ by:

$$\vec{u}(\xi^1,\xi^2,\xi^3=z,t)^{(k)}=u_i(\xi^1,\xi^2,\xi^3=z,t)^{(k)}\vec{a}^i$$

where

$$\begin{cases} u_\alpha(\xi^1,\xi^2,\xi^3=z,t)^{(k)}=\mu_\alpha^\beta v_\beta(\xi^1,\xi^2,t) \\ \quad -z\ v_{3,\alpha}(\xi^1,\xi^2,t)+F_\alpha^\beta(z)^{(k)}\gamma_\beta^0(\xi^1,\xi^2,t) \\ u_3(\xi^1,\xi^2,\xi^3=z,t)^{(k)}=v_3(\xi^1,\xi^2,t) \end{cases} \tag{6}$$

In this expression, $\gamma_\alpha^0=\beta_\alpha+b_\alpha^\beta v_\beta+v_{3,\alpha}$ are the two transverse shear strain components at the middle surface of the shell ($z=0$) and we denote by v_α the in-surface displacements, v_3 the deflexion. Notation β_α is used for rotations by convenience. It is expressed as $\beta_1=\theta_2$ and $\beta_2=-\theta_1$, where θ_1 and θ_2 are measures of the two positive rotations of the transverse shell fiber. The functions $F_\alpha^{\beta(k)}(z)$, introduced in Eq. (6), include trigonometric functions $f_1(z)$, $f_2(z)$ and linear functions $g_1^k(z), g_2^k(z)$, $g_3^k(z)$ and $g_4^k(z)$. They are defined by:

$$\begin{aligned} &F_1^{1(k)}(z)=f_1(z)+g_1{}^{(k)}(z); \quad F_1^{2(k)}z=g_2{}^{(k)}(z) \\ &F_2^{1(k)}z=g_3{}^{(k)}(z); \quad F_2^{2(k)}(z)=f_2(z)+g_4{}^{(k)}(z) \end{aligned} \tag{7}$$

with:

$$\begin{aligned} &f_1(z)=f(z)-\frac{e}{\pi}b_{55}f'(z) \\ &f_2(z)=f(z)-\frac{e}{\pi}b_{44}f'(z) \\ &g_i{}^{(k)}(z)=a_i{}^{(k)}z+d_i^{(k)} \\ &\quad i=1,2,3,4 \quad \text{and} \quad k=1,2,3,\ldots,N \end{aligned} \tag{8}$$

In Eqs. (7) and (8), $f(z)=\frac{e}{\pi}\sin\frac{\pi z}{e}$ while $f'(z)$ stands for $\frac{\partial f}{\partial z}$, e the thickness of the shell and N represents the number of layers.

Coefficients $b_{44}, b_{55}, a_i^{(k)}, d_i^{(k)}$ for $i=1,2,3,4$, introduced in Eq. (8), are determined from the boundary conditions on the top and bottom surfaces of the shell, and from the continuity requirements at each layer interfaces for displacements and transverse shear stresses, see [13] for detail calculations.

In each layer $(k)^{\text{th}}$ layer, strains and stresses are respectively denoted by $\epsilon_{ij}^{(k)}$ and $\sigma_{ij}^{(k)}$. Furthermore, the transverse normal strain ϵ_{33} is negligible according to the moderately thick shell hypothesis. The material behaviour is admitted linearly elastic and the shell lamination may be nonsymmetric and having angle ply layers.

The present Sinus model, called (SIN-C), allows analyzing effects of interlayer requirements.

Classic shell models can be derived from this formulation:

- the present Sinus model without interlayer continuity (SIN): $f_1(z)=f_2(z)=f(z)$, $g_i^{(k)}(z)=0$
- the Reissner-Mindlin–Naghdi model (RM–N): $f_1(z)=f_2(z)=z$, $g_i^{(k)}(z)=0$
- the Kirchhoff-Love–Koïter model (KL–K): $f_1(z)=f_2(z)=0$, $g_i^{(k)}(z)=0$

Hereafter, the superscript (k) for $u_\alpha^{(k)}$ components is omitted in order to lighten notations.

3.2. The strain field: general expressions

The strain tensor is expressed with respect to the contravariant base vectors $\vec{a}^i$ and after some algebraic manipulations, the strain components are deduced as:

$$\epsilon=\epsilon_{ij}(a^i\otimes a^j)$$

with

$$\begin{aligned} 2\epsilon_{\alpha\beta}=&\frac{1}{\mu}(\epsilon_{\alpha\beta}^0+\epsilon_{\beta\alpha}^0+F_\alpha^\nu(z)\epsilon_{\nu\beta}^1+F_\beta^\nu(z)\epsilon_{\nu\alpha}^1+G_\alpha^\nu(z)\epsilon_{\nu\beta}^2 \\ &+G_\beta^\nu(z)\epsilon_{\nu\alpha}^2+z\{(b_\beta^\lambda-2H\delta_\beta^\lambda)(\epsilon_{\alpha\lambda}^0+F_\alpha^\nu(z)\epsilon_{\nu\lambda}^1 \\ &+G_\alpha^\nu(z)\epsilon_{\nu\lambda}^2)+(b_\alpha^\lambda-2H\delta_\alpha^\lambda)(\epsilon_{\beta\lambda}^0+F_\beta^\nu(z)\epsilon_{\nu\lambda}^1+G_\beta^\nu(z)\epsilon_{\nu\lambda}^2)\}) \\ 2\epsilon_{\alpha3}=&\frac{1}{\mu}(F_\alpha^{\nu'}(z)\gamma_\nu^0+b_\alpha^\nu(F_\nu^\beta(z)-zF_\nu^{\beta'}(z))\gamma_\beta^0 \\ &+z(b_\alpha^\nu-2H\delta_\alpha^\nu)\{F_\nu^{\beta'}(z)\gamma_\beta^0+b_\nu^\beta(F_\beta^\lambda(z)-zF_\beta^{\lambda'}(z))\gamma_\lambda^0\}) \end{aligned} \tag{9}$$

where $G_\alpha^\nu(z)=F_\alpha^\nu(z)-\delta_\alpha^\nu z$.

By convenience, the following notations have been introduced in Eq. (9) to characterize the mechanical effects:

membrane strain: $\epsilon_{\alpha\beta}^0=v_{\alpha|\beta}-b_{\alpha\beta}v_3$,
bending strain 1: $\epsilon_{\alpha\beta}^1=\beta_{\alpha|\beta}$,
bending strain 2: $\epsilon_{\alpha\beta}^2=b_\alpha^\lambda v_{\lambda|\beta}+b_{\alpha|\beta}^\lambda v_\lambda+v_{3|\alpha\beta}$,
transverse shear strain: $\gamma_\alpha^0=\beta_\alpha+b_\alpha^\beta v_\beta+v_{3,\alpha}$,

where the notation $v_{\alpha|\beta}$ stands for the covariant derivative with respect to the ξ^β curvilinear co-ordinate.

At this stage, no assumption is carried out on the strain components: the coefficient $1/\mu$ which depends on the transverse co-ordinate z and curvature tensor components and all terms coming from the displacement field are preserved in the transverse shear strain expressions. This model is called the *complete model*.

4. The strain field simplifications

From the general strain field expressions, some simplified strain models can be expressed according to continuity requirements and geometric considerations.

4.1. SIN-C: Sin model with continuity requirements

This model is deduced from the complete one and the transverse shear strains are simplified to ensure continuity requirements:

$$
\begin{aligned}
2\epsilon_{\alpha\beta} =& \frac{1}{\mu}(\epsilon^0_{\alpha\beta} + \epsilon^0_{\beta\alpha} + F^v_\alpha(z)\epsilon^1_{v\beta} + F^v_\beta(z)\epsilon^1_{v\alpha} + G^v_\alpha(z)\epsilon^2_{v\beta} \\
&+ G^v_\beta(z)\epsilon^2_{v\alpha} + z\{(b^\lambda_\beta - 2H\delta^\lambda_\beta)(\epsilon^0_{\alpha\lambda} + F^v_\alpha(z)\epsilon^1_{v\lambda} \\
&+ G^v_\alpha(z)\epsilon^2_{v\lambda}) + (b^\lambda_\alpha - 2H\delta^\lambda_\alpha)(\epsilon^0_{\beta\lambda} + F^v_\beta(z)\epsilon^1_{v\lambda} \\
&+ G^v_\beta(z)\epsilon^2_{v\lambda})\}) \\
2\epsilon_{\alpha 3} =& F^{v'}_\alpha(z)\gamma^0_v
\end{aligned}
\tag{10}
$$

4.2. SIN-C/Love: Sin model with continuity requirements and the geometric assumptions from Love

This model takes into account the continuity conditions for the transverse shear strains and includes the following geometric assumptions: $1 \pm z b^\beta_\alpha \sim 1 \iff z b^\beta_\alpha \ll 1$. Therefore, Eq. (9) becomes:

$$
\begin{aligned}
2\epsilon_{\alpha\beta} =& \epsilon^0_{\alpha\beta} + \epsilon^0_{\beta\alpha} + F^v_\alpha(z)\epsilon^1_{v\beta} + F^v_\beta(z)\epsilon^1_{v\alpha} \\
&+ G^v_\alpha(z)\epsilon^2_{v\beta} + G^v_\beta(z)\epsilon^2_{v\alpha} \\
2\epsilon_{\alpha 3} =& F^{v'}_\alpha(z)\gamma^0_v
\end{aligned}
\tag{11}
$$

This geometric assumption, introduced by Love [14], is often called the shallow shell hypothesis in literature. In this case, only the term $v_{3|\alpha\beta}$ influences the $\epsilon^2_{\alpha\beta}$ *bending strain 2*.

4.3. SIN-C/Donnell: Sin model with continuity requirements and Donnell assumption for the transverse shear strains

Donnell's assumption consists in neglecting membrane coupling in the transverse shear strains at the middle surface. Therefore, the expression of the transverse shear strain becomes: $\gamma^0_\alpha = \beta_\alpha + v_{3,\alpha}$.

Finally, plate transverse shear strains are used in this model.

4.4. SIN-C/Love + Donnell

The strain components are those used in SIN-C/Love model with the expression of the transverse shear strain following Donnell assumption: $\gamma^0_\alpha = \beta_\alpha + v_{3,\alpha}$.

5. Comparison of different strain models on the Ren shell panel: analytical approach

5.1. The Ren cylindrical panel

The geometrical and mechanical properties of the panel presented Fig. 1 are:

Geometry: $R_{\text{moy}} = R = 10$, $\phi = 60°$, $a = R\phi$, $S = R/e = 4$, 10, 50, 100. The panel is supposed infinite along the $x_2 = \xi^2$ direction.

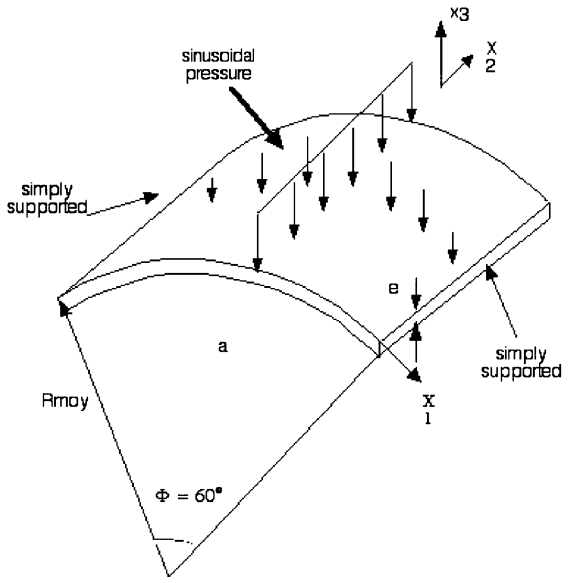

Fig. 1. The Ren laminated cylindrical shell panel.

Material properties: homogeneous or three layers of same thickness (0°, 90°, 0°) are considered using the following properties for a layer in orthotropic axes:

$$E_1 = 25E_2 \quad G_{12} = G_{13} = 0.5E_2 \quad G_{23} = 0.2E_2$$
$$\nu_{12} = 0.25$$

Loading: a single sinusoidal pressure along the curvature is imposed

$$P(\xi^1) = P_0 \sin\frac{\pi\xi^1}{R\phi}$$

Boundary conditions: the cylindrical panel is simply supported along its straight edges (see Fig. 1).

5.2. Analytical approach

In this paragraph, the bending of a cylindrical panel described above is considered using a plane strain state in the $(x_1, x_3 = z)$ plane, see Fig. 1. Therefore, from Eq. (6), the generalized displacements to be considered are: v_1, v_3 and $\beta_1 = \theta_2$ from which the strains can be deduced according to the assumptions made in Sections 4.1–4.4. For the different shell models presented above, the strain components are summarized in Table 1. In these expressions, $b^1_1 = b_{11} = -1/R$, and $\gamma^0_1 = \beta_1 + b^1_1 v_1 + v_{3,1}$ excepted for Donnell model where $\gamma^0_1 = \beta_1 + v_{3,1}$.

The boundary value problem is derived from the associated weak form as:

$$
\begin{aligned}
&\int_S \int_{-e/2}^{e/2} D^*_{11}\bar{C}_{11}\epsilon_{11}\,\mathrm{d}z\,\mathrm{d}S + \int_S \int_{-e/2}^{e/2} D^*_{13}\bar{C}_{55}2\epsilon_{13}\,\mathrm{d}z\,\mathrm{d}S \\
&+ \int_S p v^*_3\,\mathrm{d}S = 0
\end{aligned}
\tag{12}
$$

Table 1
The Ren cylindrical shell panel: the strain tensor components for different shell models

Model	Strain tensor components
Complete	$\epsilon_{11} = \frac{1}{\mu}(v_{1,1}\left(1 - \frac{F_1^1(z)}{R} + \frac{z}{R}\right) + F_1^1(z)\beta_{1,1} - b_{11}v_3 + (F_1^1(z) - z)v_{3,11})$ $2\epsilon_{13} = \frac{1}{\mu}(F_1^{1'}(z)(1 - zb_1^1)\gamma_1^0 + b_1^1F_1^1(z)\gamma_1^0) \quad \gamma_1^0 = b_1^1v_1\beta_1 + v_{3,1}$
SIN-C	$\epsilon_{11} = \frac{1}{\mu}(v_{1,1}\left(1 - \frac{F_1^1(z)}{R} + \frac{z}{R}\right) + F_1^1(z)\beta_{1,1} - b_{11}v_3 + (F_1^1(z) - z)v_{3,11})$ $2\epsilon_{13} = F_1^{1'}(z)\gamma_1^0 \quad \gamma_1^0 = b_1^1v_1 + \beta_1 + v_{3,1}$
SIN-C/Love	$\epsilon_{11} = v_{1,1} + F_1^1(z)\beta_{1,1} - b_{11}v_3 + (F_1^1(z) - z)v_{3,11}$ $2\epsilon_{13} = F_1^{1'}(z)\gamma_1^0 \quad \gamma_1^0 = b_1^1v_1 + \beta_1 + v_{3,1}$
SIN-C/Donnell	$\epsilon_{11} = \frac{1}{\mu}(v_{1,1}\left(1 - \frac{F_1^1(z)}{R} + \frac{z}{R}\right) + F_1^1(z)\beta_{1,1} - b_{11}v_3 + (F_1^1(z) - z)v_{3,11})$ $2\epsilon_{13} = F_1^{1'}(z)\gamma_1^0 \quad \gamma_1^0 = \beta_1 + v_{3,1}$
SIN-C/Love-Donnell	$\epsilon_{11} = v_{1,1} + F_1^1(z)\beta_{1,1} - b_{11}v_3 + (F_1^1(z) - z)v_{3,11}$ $2\epsilon_{13} = F_1^{1'}(z)\gamma_1^0 \quad \gamma_1^0 = \beta_1 + v_{3,1}$

where D_{11}^* and D_{13}^* stand for the virtual strain rate and $\bar{C}_{11}$, $\bar{C}_{55}$ are the bidimensional elastic moduli of the material, taking into account the zero transverse normal stress assumption $\sigma_{33} = 0$.

The closed form solution is deduced introducing the generalized displacements under the following form:

$$\begin{cases} v_1 = V_1 \cos(\lambda s) \\ \beta_1 = \beta \cos(\lambda s) \\ v_3 = V_3 \sin(\lambda s) \end{cases} \tag{13}$$

which satisfies both the boundary conditions and the equilibrium equations derived from Eq. (12). $\lambda = \frac{3}{R}$ and s stands for ξ^1 in the above expressions.

5.3. The homogeneous case

This section deals with the homogeneous Ren panel case [15] and two numerical evaluations are conducted: the first one is dedicated to the influence of the $1/\mu$ approximation and the second one deals with an evaluation of the previous shell models on the homogeneous Ren cylindrical shell panel.

5.3.1. Influence of $1/\mu$ approximation

For the SIN-C model, the influence of various approximations on the factor $1/\mu$ function of the coordinate z, is studied.

Table 2 presents results obtained with three kinds of approximation: first, third and fifth order development of $1/\mu(z)$. Nondimensionalized normal transversal displacement v_3, membrane/bending stress σ_{11} and transverse shear stress σ_{13}, as in [15], are given for different ratios $S = \frac{R}{e}$. We can observe that the solution is not significantly improved when the degree of approximation increases. Therefore, in order to simplify analytical calculations, the first order approximation for $1/\mu$ factor is kept.

Table 2
The Ren multilayered cylindrical shell panel: influence of $1/\mu$ approximation

Ratio S	$1/\mu$ approximation	v_3	σ_{11}	σ_{13}
$S=4$	3D elasticity	0.312	1.079	0.572
	1st order	0.276	0.969	0.554
	3rd order	0.275	0.977	0.553
	5th order	0.275	0.977	0.553
$S=10$	3D elasticity	0.115	0.807	0.579
	1st order	0.108	0.769	0.576
	3rd order	0.108	0.769	0.576
	5th order	0.108	0.769	0.576
$S=50$	3D elasticity	0.0770	0.752	0.568
	1st order	0.0762	0.745	0.580
	3rd order	0.0762	0.745	0.580
	5th order	0.0762	0.745	0.580
$S=100$	3D elasticity	0.0755	0.751	0.565
	1st order	0.0752	0.747	0.580
	3rd order	0.0751	0.747	0.580
	5th order	0.0751	0.747	0.580

The models introduced in the above section with strain components given in Table 1 are now evaluated using the first order approximation excepted for the SIN-C/Love one which is based on the assumption $1 \pm zb_\alpha^\beta \sim 1$.

5.3.2. Analytical results for different shell models

Based on the Ren cylinder test described in Section 5.1, this part permits to evaluate the behaviour of the different shell models, described above in Sections 4.1–4.4.

Nondimensionalized results for $v_3, \sigma_{11}, \sigma_{13}$ are summarized in Table 3. In this table, ratio $S = R/e = 4$ is very constraining because the validity of a shell model can be

Table 3
The Ren cylindrical shell panel: analytical nondimensionalized displacements and stresses

S ratio	Model	v_3	σ_{11}	σ_{13}
4	3D elasticity	0.312	1.079	0.572
	SIN-C	0.277	0.971	0.557
	SIN-C/Love	0.260	1.096	0.537
	SIN-C/Donnell	0.232	0.876	0.512
	SIN-C/Love+Donnell	0.219	0.986	0.495
10	3D elasticity	0.115	0.807	0.579
	SIN-C	0.108	0.769	0.576
	SIN-C/Love	0.102	0.795	0.560
	SIN-C/Donnell	0.090	0.695	0.527
	SIN-C/Love+Donnell	0.085	0.719	0.512
50	3D elasticity	0.0770	0.752	0.568
	SIN-C	0.0762	0.745	0.580
	SIN-C/Love	0.0720	0.742	0.563
	SIN-C/Donnell	0.0633	0.670	0.529
	SIN-C/Love+Donnell	0.0602	0.668	0.516
100	3D elasticity	0.0755	0.751	0.565
	SIN-C	0.0751	0.747	0.580
	SIN-C/Love	0.0711	0.741	0.563
	SIN-C/Donnell	0.0624	0.671	0.530
	SIN-C/Love+Donnell	0.0594	0.667	0.516

discussed. Nevertheless, we can observe a good agreement for this ratio with reference values.

SIN-C/Donnell and SIN-C/Love+Donnell models are very penalyzing for both transverse displacement and stresses due to the transverse shear strain expression, see Sections 4.3 and 4.4.

For the SIN-C/Love model, relative error in comparison with SIN-C model varies from 6.5% to 5.5% for the transverse displacement and from 3.6% to 2.7% for the transverse shear stress. Moreover, SIN-C/Love overestimates the normal transverse stress in comparison with SIN-C model.

From Table 3, the more homogeneous results for deflexion and stresses are obtained with the SIN-C model, which is used later in this paper.

5.4. The multilayered case

SIN, SIN-C and RM–N, for Reissner-Mindlin–Naghdi, models (see Section 3.1) are now evaluated in the case of the multilayered Ren cylindrical panel with geometrical and mechanical properties as given in Section 5.1. Results on this evaluation are summarized in Table 4. The first order approximation for $1/\mu$ is conserved as discussed above.

The efficiency of the SIN-C model which takes into account continuity requirements for the displacement and for the transverse shear stresses, and does not need any shear correction factor, is obvious in Table 4. Distribution of the transverse shear stress σ_{13} is shown on Fig. 2 where continuous lines stand for interlayers.

Table 4
The Ren multilayered cylindrical shell panel: nondimensionalized displacements and stresses

Ratio S	Model	v_3	σ_{11}	σ_{13}
4	3D elasticity	0.457	1.772	0.476
	SIN-C	0.399	1.293	0.460
	SIN	0.385	1.139	0.343
	RM–N	0.339	0.680	0.186
10	3D elasticity	0.144	0.995	0.525
	SIN-C	0.136	0.860	0.525
	SIN	0.129	0.822	0.359
	RM–N	0.120	0.739	0.187
50	3D elasticity	0.0808	0.798	0.526
	SIN-C	0.0800	0.775	0.539
	SIN	0.0796	0.774	0.362
	RM–N	0.0792	0.770	0.187
100	3D elasticity	0.0787	0.786	0.523
	SIN-C	0.0782	0.775	0.540
	SIN	0.0781	0.775	0.362
	RM–N	0.0779	0.774	0.187

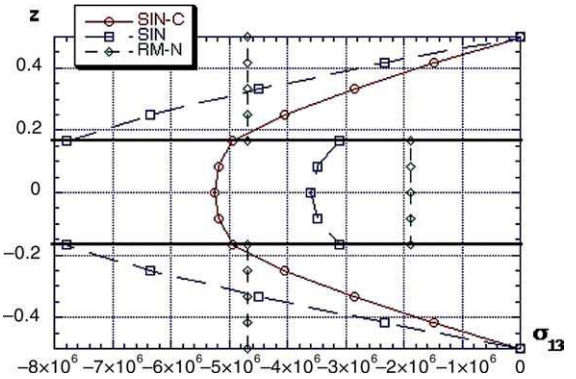

Fig. 2. The Ren laminated cylindrical shell panel: distribution of the transverse shear stress σ_{13}.

6. The triangular six node finite element

The discrete formulation of the boundary value problem for shells is deduced from the standard functional:

$$a(\vec{u}^h, \vec{u}^{*h})_{\cup\Omega_e} = f(\vec{u}^{*h})_{\cup\Omega_e} + F(\vec{u}^{*h})_{\cup\mathscr{C}_e}, \quad \forall \vec{u}^{*h} \tag{14}$$

In Eq. (14), $\cup\Omega_e$ is the triangulation of the multilayered structure and $\cup\mathscr{C}_e$ is its edges. In addition, $\vec{u}^h$ is the

finite element approximation of the displacement field $\vec{u}$ given by Eq. (6) and $\vec{u}^{*h}$ is the finite element approximation of the corresponding virtual velocity field $\vec{u}^{*}$. Linear functions f and F represent the body (including inertia terms) and surface loads. The superscript h introduced in Eq. (14) which indicates the finite element approximation, is also used for the finite element approximation of the generalized displacements v_i^h and θ_α^h defined in Eq. (6).

6.1. The finite element approximations

The geometry is approximated using the classic linear three node triangle. The geometrical transformation using an explicit map $\vec{\Phi}$ is illustrated in Fig. 3.

In a conforming finite element approach, the displacement field, given by Eq. (6) requires that v_3 has to be approximated by a C^1-continuous function, while the other generalized displacements v_α and θ_α require a C^0-continuous.

Therefore, Argyris [16] finite element approximation is used for the deflexion and Ganev [17] for the other generalized displacements. Note that the Argyris interpolation is exactly of continuity C^1 and the Ganev interpolation involves a semi-C^1 continuity.

The degrees of freedom (dof) associated with this kind of finite element in the local curvilinear base vectors are:

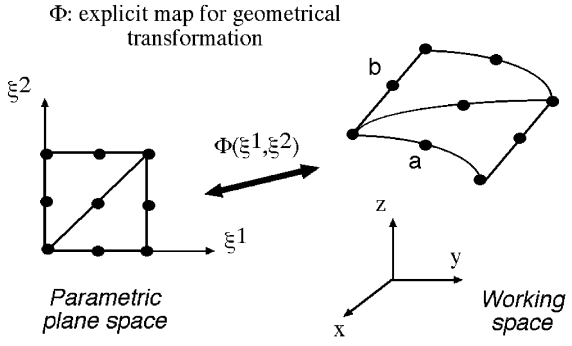

Fig. 3. Geometrical transformation using explicit map.

- at a corner node:

$$\begin{array}{cccccc} v_1 & v_{1,1} & v_{1,2} & v_2 & v_{2,1} & v_{2,2} \\ v_3 & v_{3,1} & v_{3,2} & v_{3,11} & v_{3,22} & v_{3,12} \\ \theta_1 & \theta_{1,1} & \theta_{1,2} & \theta_2 & \theta_{2,1} & \theta_{2,2} \end{array} \tag{15}$$

- at a mid-side node:

$$\begin{array}{cccc} v_1 & v_{1,n} & v_2 & v_{2,n} \\ v_{3,n} & & & \\ \theta_1 & \theta_{1,n} & \theta_2 & \theta_{2,n} \end{array} \tag{16}$$

where $p_{,n}$ is the derivative of $p=(v_i,\theta_\alpha)$ with respect to the normal direction n of the edge of the element

Then, having derivatives in the previous set of degrees of freedom, the following methodology is used to prescribe kinematic boundary conditions for the previous derivative degree of freedom (dof).

For a given p function and a boundary condition such that $p(\xi^1=0,\xi^2)=0,\ \forall\xi^2$, the first order derivatives can be expressed using the derivative definition:

$$\begin{aligned} p_{,1}(0,\xi^2) &= \lim_{h\to 0}\frac{p(h,\xi^2)-p(0,\xi^2)}{h} \neq 0 \\ p_{,2}(0,\xi^2) &= \lim_{h\to 0}\frac{p(0,\xi^2+h)-p(0,\xi^2)}{h} = 0 \end{aligned} \tag{17}$$

The same procedure can be used for the second order derivative dof and Table 5 gives the synthesis of the prescribed dof for Argyris and Ganev finite element approximations. In this table, 0 indicates that the degree of freedom must be fixed, while 1 means that it is free. When the degree of freedom does not exist, we write –.

6.2. The elementary matrices

6.2.1. Elementary stiffness matrix

The elementary stiffness matrix $[K_e]$ is obtained by computing the bilinear form given in Eq. (14) at the elementary level as:

$$\begin{aligned} a(\vec{u}^h,\vec{u}^{*h})_{\Omega_e} &= \int_{\Omega_e}\int_{-e/2}^{e/2}\left[\epsilon_e^{*h}\right]^{\mathrm{T}}\left[\bar{C}^{(k)}\right]\left[\epsilon_e^h\right]\mu\,\mathrm{d}z\sqrt{a}\,\mathrm{d}\Omega_e \\ &= \int_{\Omega_e}\left[E_e^{*h}\right]^{\mathrm{T}}\left(\int_{-e/2}^{e/2}[B_e]^{\mathrm{T}}\left[\bar{C}^{(k)}\right][B_e]\mu\,\mathrm{d}z\right)\left[E_e^h\right]\sqrt{a}\,\mathrm{d}\Omega_e \\ &= \int_{\Omega_e}\left[E_e^{*h}\right]^{\mathrm{T}}[A_e]\left[E_e^h\right]\sqrt{a}\,\mathrm{d}\Omega_e = \left[Q_e^*\right]^{\mathrm{T}}[K_e][Q_e] \end{aligned} \tag{18}$$

Table 5
Boundary conditions values for a given p function using Ganev or Argyris interpolations

Edge	Interpolation	p	$p_{,1}$	$p_{,2}$	$p_{,n}$	$p_{,11}$	$p_{,22}$	$p_{,12}$
$\xi^1=$cste	GANEV	0	1	0	1	–	–	–
	ARGYRIS	0	1	0	1	1	0	1
$\xi^2=$cste	GANEV	0	0	1	1	–	–	–
	ARGYRIS	0	0	1	1	0	1	1

To develop Eq. (18), the classic orthotropic elastic constitutive law, using matrix notation, has been introduced as:

$$[\sigma_e^h] = [\bar{C}^{(k)}][\epsilon_e^{*h}] \tag{19}$$

where $[\sigma_e^h]$ is the matrix of stress components and $[\bar{C}^{(k)}]$ the matrix associated with the bidimensional moduli of the material for the k^{th} layer taking into account of the zero transverse normal stress hypothesis.

Using the displacement field $\vec{u}$ in Eq. (6) and the strains defined in Eq. (9), the matrix $[B_e]$ can easily be deduced and contains all the functions depending on z co-ordinate. The matrix $[E_e^h]$, identically for $[E_e^{*h}]$ adding the asterisk superscript, which may be seen as a generalized strain matrix is given by:

$$[E_e^h]^{\mathrm{T}} = [v_1^h\ v_{1,1}^h\ v_{1,2}^h \vdots v_2^h\ v_{2,1}^h\ v_{2,2}^h \vdots v_3^h\ v_{3,1}^h\ v_{3,2}^h\ v_{3,11}^h\ v_{3,12}^h\ v_{3,22}^h \vdots \theta_1^h\ \theta_{1,1}^h\ \theta_{1,2}^h \vdots \theta_2^h\ \theta_{2,1}^h\ \theta_{2,2}^h] \tag{20}$$

The finite element approximations, defined at the above Section 6.1, are directly used to express the matrix $[E_e^h]$ as a function of the degrees of freedom vector $[Q_e]$ at the element level (see Eqs. (18) and (20)).

Finally, $[A_e]$ contains the linearly elastic material behaviour matrix for a multilayered shell which results on the integration with respect to the thickness co-ordinate.

6.2.2. Elementary mass matrix

The consistent elementary mass matrix $[M_e]$ is immediately computed, using the same method as for the stiffness one, and we have:

$$\int_{\Omega_e}\int_{-e/2}^{e/2} \rho_e [u^{*h}]^{\mathrm{T}}[\ddot{u}^h]\mu\,\mathrm{d}z\sqrt{a}\,\mathrm{d}\Omega_e = [Q_e^*]^{\mathrm{T}}[M_e][\ddot{Q}_e] \tag{21}$$

In this equation, $(\ddot{}) = \partial^2(\ )/\partial t^2$ and ρ_e is the mass density of the element Ω_e.

Finally, the load vector is similarly deduced and there is no need to develop its expression.

All the elementary matrices presented here are exactly integrated using 16 points.

7. Numerical evaluations

This new finite element has already been evaluated on classical shell tests for homogeneous shell structures [18] and very good results have been obtained but no detail is given here. This section is dedicated to numerical evaluations of this new finite element on multilayered structures.

The aim of the numerical tests is to characterize accuracy and convergence properties for both displacements and stresses for some multilayered shells where reference solutions are available. As indicated before (see Section 3), the Sinus model with continuity requirements (SIN-C) permits recovering other classical models specifying expressions for $f_\alpha(z)$ and $g_i(z)^{(k)}$ for $i=1$, 4. Numerical developments associated to the present six node triangular finite element, denoted GAG (for Ganev–Argyris–Ganev finite element approximations), give the opportunity to compare various models.

7.1. Static linear test on a cylindrical shell panel

Numerical results are presented in this section for a simply supported cross-ply cylindrical shell panel, see Fig. 4. The geometry of this cylindrical panel is defined by means of its radius R, its length b, its circumferential length a. Geometrical, material and loading properties have been chosen as follows:

Geometry: $R=10$, ratio $b/a=3$ and two ratios $R/a=1$, 4 defining respectively deep and shallow shells are considered. The thickness e is defined by means of two ratios $a/e=5$, 10.

Boundary conditions and loading: this cross-ply cylindrical shell panel is simply supported at its edges, and is subjected to a transverse doubly sinusoidal load.

Material properties: the shell has got three layers (0°, 90°, 0°) of equal thickness and the lamina material properties are taken from Ref. [19] and given in Section 5.1.

Results: the mesh $N=4$ with 760 dof is used and results are given for $v_3(a/2, b/2, 0)$; $\sigma_{11}(a/2, b/2, -e/2)$; $\sigma_{22}(a/2, b/2, e/6)$; $\sigma_{12}(0, 0, -e/2)$; $\sigma_{13}(0, b/2, 0)$; $\sigma_{23}(a/2, 0, 0)$.

The first result is about the convergence velocity of the present element. Relative deviations for deflexion and stresses with respect to the 3D elasticity solution [20] are plotted in Fig. 5 versus the number of degree of freedom (dof). This Figure shows the convergence efficiency of the present element. The converged values are quickly reached for global transverse displacement v_3 at the center of the shell panel: deviation is 0.85% with

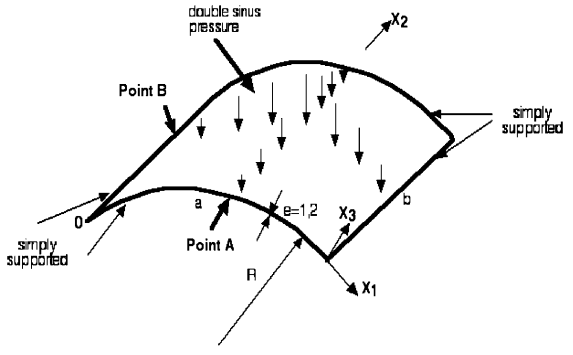

Fig. 4. Three layers cylindrical panel under transverse doubly sinusoidal pressure.

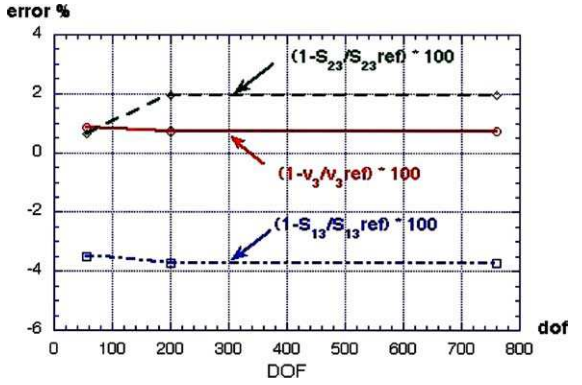

Fig. 5. Convergence study for deflexion and stresses with respect to 3D elasticity solutions.

55 dof and 0.75% with 200 dof. For local quantities such as transverse shear stresses σ_{13} and σ_{23}, respectively located at $(0, b/2, 0)$ and $(a/2, 0, 0)$, relative error never exceeds 4 with a very coarse mesh using the present finite element.

Numerical results obtained with the present finite element (mesh $N=4$, 760 dof) are compared in Table 6 with the elasticity solution given by Huang [20].

Results from the present finite element are in good agreement with elasticity solutions for both transverse displacement and stresses, and the effect of the continuity condition is very significant. For the most difficult case, $R/a=1$ and $a/e=5$ which is a deep thick shell, numerical results present the following deviations in comparison to the elasticity solution: $-6.\%$ for the transverse displacement, $(3., -7., -5.)\%$ for the stresses $(\sigma_{11}, \sigma_{22}, \sigma_{12})$, and finally $(-2., -12)\%$ for the transverse shear stresses $(\sigma_{13}, \sigma_{23})$.

7.2. Free vibration tests

A simply supported two-layer cross-ply cylindrical panel is considered and the first dimensionless natural frequency is compared with an analytical value given in [21]. Characteristics of this cylindrical panel are as follows:

Geometry: a rectangular shell with $R=4.$, $a=2.$ and different ratios $L/a=1$, 2, 3, 4, 5 are considered, where L is the straight edge length. The thickness is given by $e=0.1$.

Boundary conditions: this cross-ply cylindrical shell panel is simply supported at its edges.

Material properties: two layers (0°, 90°) of equal thickness are considered and the lamina material properties are taken from [19] given above in Section 5.1.

Results: the lowest frequency parameter is given.

Results shown in Table 7 are in good agreement with the reference solution. One can observe that the Kirchhoff-Love–Koïter (KL–K) model overestimates the first natural frequency for all the ratios while RM–N model underestimates this natural frequency. Deviations with respect to the analytical solution never exceed 2%.

Table 7
Free vibrations of a simply supported two layers cylindrical panel. First flexural eigen frequency and comparison with an analytical solution

L/a	Ref. [21]	SIN-C	KL–K	RM–N
1	11.71	11.66	11.74	11.54
2	7.35	7.28	7.42	7.24
3	6.58	6.49	6.65	6.43
4	6.32	6.23	6.40	6.19
5	6.22	6.11	6.28	6.08

Table 6
The simply supported cross-ply cylindrical shell panel: nondimensionalized displacements and stresses

R/a	a/e	Models	$\bar{v}_3$	$\bar{\sigma}_{11}$	$\bar{\sigma}_{22}$	$\bar{\sigma}_{12}$	$\bar{\sigma}_{13}$	$\bar{\sigma}_{23}$
1	5	Elas.	2.716	−1.293	2.411	0.4371	0.4447	0.3442
		SIN-C	2.551	−1.250	2.239	0.4151	0.4352	0.3020
		SIN	2.193	−1.016	1.927	0.3563	0.3072	0.3187
1	10	Elas.	1.153	−0.8534	1.602	0.2725	0.4697	0.1848
		SIN-C	1.168	−0.8638	1.617	0.2799	0.4803	0.1819
		SIN	0.982	−0.7498	1.365	0.2376	0.3143	0.1891
4	5	Elas.	2.118	−1.022	1.116	0.2588	0.3867	0.2729
		SIN-C	2.048	−1.043	1.079	0.2508	0.4048	0.2489
		SIN	1.937	−0.923	1.024	0.2358	0.2930	0.2858
4	10	Elas.	0.9396	−0.7463	0.6468	0.1510	0.4271	0.1555
		SIN-C	0.9318	−0.7432	0.6415	0.1494	0.4434	0.1524
		SIN	0.8763	−0.7026	0.6076	0.1412	0.3029	0.1734

7.3. Transient response

Implicit and explicit time integration schemes have been implemented to evaluate the behaviour in dynamics of this new finite element. Some tests have been performed on homogeneous plates and finally on multilayered shells. Parametric studies such as sensitivity to the time integration on the transient response or damping factor influence on the dynamic behaviour have been accomplished valiading the implementation. Uniform pressure and Dirac loading have been tested on simply supported cylindrical shell panel. The results obtained under Dirac loading are presented here.

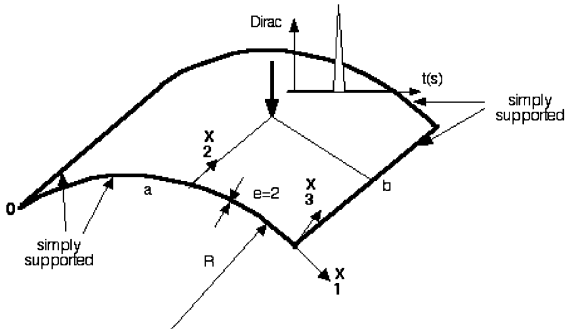

Fig. 6. Laminated cylindrical panel for dynamic tests.

Geometrical and material characteristics of this cylindrical panel, see Fig. 6, are as follows:

Geometry: a rectangular shell with $R=10.$, ratio $b/a=3.$ and ratio $R/a=1$, is considered. Ratio $a/e=10$ is used in this case.

Boundary conditions and loading: this cross-ply cylindrical shell panel is simply supported at its edges, and is subjected to an impulsive normal load at its center.

Material properties: the shell has got three layers $(0°, 90°, 0°)$ of equal thickness and the lamina material

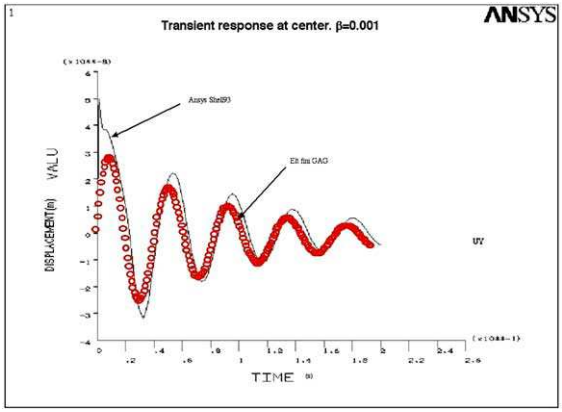

Fig. 7. Compared response with numerical simulation from Ansys.

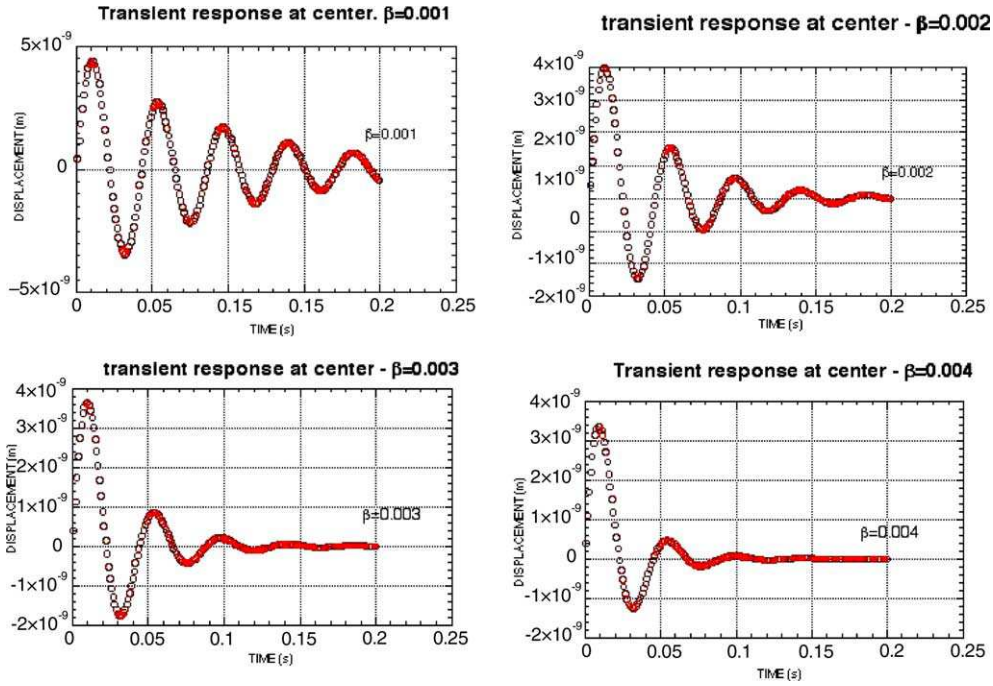

Fig. 8. Transient response of cylindrical panel under impulsive excitation on its center. Arbitrary Rayleigh damping is used.

properties are taken from Pagano [19] given above in Section 5.1.

Transient responses have been achieved on this multilayered panel. For each simulation, the results are in good agreement in comparison with 3D solid or shell finite element computations from Ansys Software [22].

The transient responses given by the present element and Shell93 element from Ansys Sofware are compared in Fig. 7. For this simulation, the arbitrary Rayleigh damping factor value is $\beta = 0.001$. A good agreement for the global dynamic responses of the panel is observed. On the other hand, Fig. 8 shows the evolution of the dynamic response when arbitrary Rayleigh damping factor increases. Responses are in agreement with theoretical results again. Finally, these first investigations in dynamics are very encouraging for future work, especially for impacts and damage studies in dynamics.

8. Conclusions

In this paper, a new triangular finite element has been presented to analyze multilayered shells in static and dynamic.

A discussion on various assumptions at the strain level was firstly presented in order to clarify the influence of classical strain simplifications and truncatures. The refined shell theory used, which contains only five independent generalized displacements, allows satisfying exactly all the boundary conditions at the top and bottom surfaces of the shell and the interlaminar continuity for displacement and stresses. Furthermore, this shell model involves nonlinear distributions displacements and stresses, avoiding the use of transverse shear correction factors.

On the other hand, a conforming finite element method has been used to define a new finite element based on higher-order polynomia approximations for the generalized displacements. Several tests have shown its efficiency for both convergence velocity and accuracy for displacements and stresses.

Present works have recently been followed by the introduction of a moderately large transverse displacement (Von-Karmann assumptions) for geometrically nonlinear applications.

References

[1] Noor A, Burton W, Bert C. Computational models for sandwich panels and shells. App Mech Rev 1996;49(3):155–99.

[2] Reddy J, Liu C. A higher-order shear deformation theory of laminated elastic shells. Int J Eng Sci 1985;23:319–30.

[3] Touratier M. A refined theory of laminated shallow shells. Int J Solids Struct 1992;29(11):1401–15.

[4] He L-H. A linear theory of laminated shells accounting for continuity of displacements and transverse shear stresses at layer interfaces. Int J Solids Struct 1994;31(5):613–27.

[5] Sciuva MD. A third order triangular multilayered plate finite element with continuous interlaminar stresses. Int J Numer Methods Eng 1995;38:1–26.

[6] Shu X-P. A refined theory of laminated shells with higher order transverse shear deformation. Int J Solids Struct 1997;34(6):673–83.

[7] Ossadow C, Touratier M, Muller P. Deep doubly curved multilayered shell theory. AIAA J 1999;37(1):100–9.

[8] Carrera E. Multilayered shells theories accounting for layerwise mixed description, part 1: governing equations. AIAA J 1999;37(9):1107–16.

[9] Botello S, Onate E, Canet J. A layer-wise triangle for analysis of laminated composite plates and shells. Comput Struct 1999;70:635–46.

[10] Klinkel S, Gruttmann F, Wagner W. A continuum based three dimensional shell element for laminated structures. Comput Struct 1999;71:43–62.

[11] Polit O, Touratier M. High order triangular sandwich plate finite element for linear and nonlinear analyses. Comput Methods Appl Mech Eng 2000;185:305–24.

[12] Bernadou M. Finite element methods for thin shell problems. John Wiley & Sons; 1996.

[13] Béakou A, Touratier M. A rectangular finite element for analysing composite multilayered shallow shells in statics, vibration and buckling. Int J Numer Methods Eng 1993;36:627–53.

[14] Love A. A treatise on the mathematical theory of elasticity. Fourth ed. New York: Dover Publications; 1944.

[15] Ren JG. Exact solutions for laminated cylindrical shells in cylindrical bending. Comput Sci Tech 1987;29:169–87.

[16] Argyris J, Fried I, Scharpf D. The tuba family of plate elements for the matrix displacement method. Aero J Royal Aeronaut Soc 1968;72:701–9.

[17] Ganev H, Dimitrov T. Calculation of arch dams as a shell using an IBM-370 computer and curved finite elements. In: Theory of shells. Amsterdam: North-Holland; 1980. p. 691–6.

[18] Batoz J, Dhatt G. Modelling of structures by finite elements. Paris: Hermès; 1992. [in French].

[19] Pagano N. Exact solutions for rectangular bidirectional composites and sandwich plates. J Comput Mater 1970;4:20–34.

[20] Huang NN. Influence of shear correction factors in the higher order shear deformation theory. Int J Solids Struct 1994;31(9):1263–77.

[21] Bert C, Kumar M. Vibration of cylindrical shells of bimodulus composite materials. J Sound Vib 1982;81(1):107–21.

[22] Ansys, Ansys Theoretical Manual V6.0, Swanson Analysis Inc, 2002.